

# Manipulating Superparamagnetic Microparticles with an Electromagnetic Needle

Zoran Cenev, Hongbo Zhang,\* Veikko Sariola, Antti Rahikkala, Dongfei Liu, Hélder A. Santos,\* and Quan Zhou\*

Selective, precise, and high-throughput manipulation of individual superparamagnetic microparticles has profound applications in performing location-tailored *in vitro* biomedical studies. The current techniques for manipulation of microparticles allow only a single particle in the manipulation workspace, or simultaneous transportation of multiple microparticles in batches. In this work, a method based on a robotized electromagnetic needle for manipulation of individual superparamagnetic microparticles within a microparticle population is introduced. By automatically controlling the highly localized magnetic field of the needle, a single microparticle is selectively picked when its neighboring particle is few micrometers away. Supported by the nanometer resolution of the robotic positioner, particles are placed at sub-micrometer precision. This manipulation technique allows the creating of arbitrary patterns, sorting of microparticles based on size and morphology, and transporting of individual microparticles in 3D space. Therefore, this approach has the potential to enable more deterministic and quantitative microanalysis and microsynthesis using superparamagnetic microparticles.

organisms. The manipulation of superparamagnetic microparticles, in particular, has a wide range of applications, including magnetic logic;<sup>[13]</sup> sorting and trapping of magnetically tagged proteins,<sup>[14]</sup> cells,<sup>[15]</sup> and microorganisms;<sup>[16]</sup> microfluidic mixing;<sup>[17]</sup> magnetoresistive biosensing;<sup>[18]</sup> immunoassays;<sup>[19]</sup> and lab-on-a-tube devices.<sup>[20]</sup> In principle, the manipulation methods of these microparticles can be categorized into two groups: batch and individual particle manipulation. In batch manipulation, the magnetic field and field gradient originate from sources, such as external permanent magnet,<sup>[19]</sup> micropatterned current wires,<sup>[21,22]</sup> and microfabricated arrays of permanent magnets.<sup>[23]</sup> These systems are usually coupled with fluidic flows within fluidic chips. The microparticles are treated collectively as a lot with the manipulation strategies being mainly

## 1. Introduction


Objects at the micro- and nanometer scale have been manipulated using mechanical force,<sup>[1–3]</sup> optical,<sup>[4–6]</sup> magnetic,<sup>[7,8]</sup> acoustic,<sup>[9,10]</sup> and electrostatic fields<sup>[11,12]</sup> for position and orientation control of particles, rods, fluidic drops, or even living

limited to trapping, separation (e.g., magnetic from nonmagnetic particles) or unidirectional transportation.<sup>[24]</sup>

The individual particle manipulation, on the contrary, allows 1D, 2D, and 3D positioning, as well as possible orientation control of an individual magnetic microparticle. 1D transportation has been carried out by serpentine microcurrent lines<sup>[25]</sup> or by zig-zag

Z. Cenev, Prof. Q. Zhou  
Department of Electrical Engineering and Automation  
School of Electrical Engineering  
Aalto University  
Maarintie 8, FI-00076 Espoo, Finland  
E-mail: quan.zhou@aalto.fi

Prof. H. Zhang  
Department of Pharmaceutical Science  
Åbo Akademi University  
Artillerigatan 6, FI-02520 Turku, Finland  
E-mail: hongbo.zhang@abo.fi

 The ORCID identification w(s) for the author(s) of this article can be found under <https://doi.org/10.1002/admt.201700177>.

© 2017 The Authors. Published by WILEY-VCH Verlag GmbH & Co. KGaA, Weinheim. This is an open access article under the terms of the Creative Commons Attribution-NonCommercial License, which permits use, distribution and reproduction in any medium, provided the original work is properly cited and is not used for commercial purposes.

The copyright line of this paper was changed 10 November 2017 after initial publication.

DOI: 10.1002/admt.201700177

Prof. V. Sariola  
Faculty of Biomedical Sciences and Engineering  
Tampere University of Technology  
FI-33720 Tampere, Finland  
Dr. A. Rahikkala  
Drug Research Program  
Division of Pharmaceutical Chemistry and Technology  
Faculty of Pharmacy  
University of Helsinki  
Viikinkaari 5E, FI-00014 Helsinki, Finland  
Dr. D. Liu, Prof. H. A. Santos  
Drug Research Program  
Division of Pharmaceutical Chemistry and Technology  
Faculty of Pharmacy  
University of Helsinki  
Viikinkaari 5E, FI-00014 Helsinki, Finland  
E-mail: helder.santos@helsinki.fi  
Dr. D. Liu, Prof. H. A. Santos  
Helsinki Institute of Life Science (HiLIFE)  
University of Helsinki  
FI-00014 Helsinki, Finland

micropatterned domain walls.<sup>[26–28]</sup> Electro-magnetic needles<sup>[29–31]</sup> have also been used for 1D magnetophoretic attraction and 2D guiding of superparamagnetic microparticles, as well as DNA stretching. Other, 2D transportation with potential rotation of microparticles has been achieved by micropatterned thin film magnetic elements<sup>[32]</sup> and current wires,<sup>[33]</sup> two-pair electromagnets,<sup>[34]</sup> as well as magneto-optical tweezers.<sup>[35,36]</sup> The systems using micropatterned elements are usually coupled with an external magnetic field coming from a permanent magnet,<sup>[25]</sup> single,<sup>[33]</sup> or two pair Helmholtz coils<sup>[26–28]</sup> or electromagnets.<sup>[32]</sup> In addition, multipole solenoids enable 3D positioning.<sup>[37,38]</sup>

Most of these techniques allow only one microparticle in the manipulation workspace, and none of them has demonstrated precise 2D/3D positioning of individual particles when multiple superparamagnetic microparticles are present in the manipulation area. This kind of manipulation approach can be beneficial in cell studies where extracting a particle from a population and delivering it to a specific location is required (e.g., onto a cellular membrane).

In this paper, we present precise 2D and 3D manipulation of individual superparamagnetic microparticles within a population of particles using an electromagnetic needle and a robotic positioner. We employ programmed magnetophoresis for selective picking of individual microparticles. The particle placement is based on the particle to substrate adhesion overcoming the adhesion between the particle and the needle. Our method can be used to selectively pick individual superparamagnetic microparticles from a population of particles, and precisely place them at a desired location without disturbing particles placed nearby. We create arbitrary patterns at sub-micrometer precision, perform particle sorting based on the size and morphology of the particles, and achieve precise positioning on 3D surfaces.

## 2. Results and Discussion

### 2.1. Concept of Manipulating Individual Superparamagnetic Microparticles

The manipulation device is an electromagnetic needle (Figure 1a), which is essentially a coil wrapped around an electrochemically sharpened surgical grade martensitic stainless steel wire with tip radius  $\approx 2 \mu\text{m}$ . The needle is attached to a robotic nanopositioner and installed within an inverted microscope (Experimental Section). The manipulated microparticles (mean diameter of  $6.85 \pm 0.50 \mu\text{m}$ ) are made of hypromellose acetate succinate (HPMCAS) encapsulating iron-III-oxide nanoparticles ( $\text{Fe}_3\text{O}_4@$ HPMCAS).<sup>[39]</sup> The microparticles are immersed in deionized

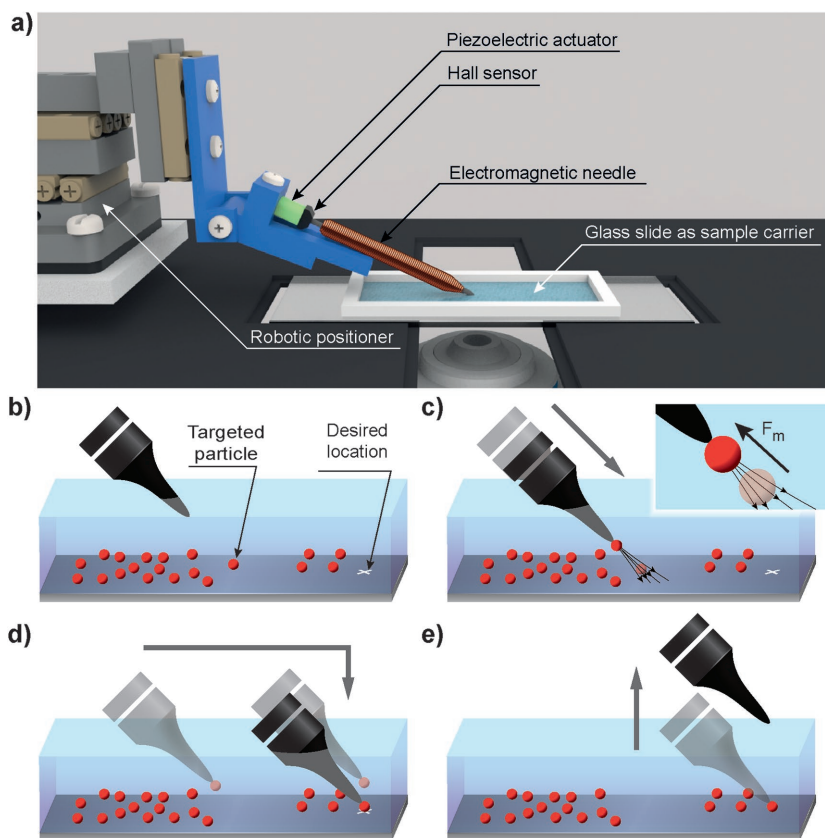


**Figure 1.** Concept for manipulating individual superparamagnetic microparticles. Illustration not to scale. a) Schematic of the manipulation device and experimental environment. b) Initial state: electromagnetic needle and two distinct populations of superparamagnetic microparticle immersed in DI water. Targeted particle is to be transported to its desired location (denoted with white cross). c) Electromagnetic needle is brought closer to the particle (gray arrow denotes the direction of the movement) and once magnetized, it picks up the targeted microparticle. Inset: close-up of the magnetophoretic picking of the microparticle. d) Microparticle transportation by the aid of the robotic positioner and its placement on the targeted location onto the substrate. e) Particle has been brought into contact with the substrate and the needle is retracted, while the particle remains adhered to the substrate.

(DI) water residing on the surface of a microscopic glass slide as sample carrier. Figure 1b shows the initial state of the manipulation process, where a targeted particle and its desired location are emphasized. The manipulation starts with the robotic positioner bringing the needle near the targeted particle. By applying a carefully programmed current to the coil, a highly localized magnetic field is generated at the vicinity of the needle tip, which attracts the microparticle toward it (Figure 1c). Once the particle is picked up, the electromagnetic needle is demagnetized and the particle is transported to the desired location (Figure 1d). When the particle encounters the substrate, the needle is pulled away and the particle is left on the substrate due to higher particle-to-substrate adhesion (Figure 1e). Experimental validation of the manipulation method is further elaborated in Video S1 (Supporting Information).

### 2.2. Magnetic Characterization

To estimate the magnetic forces acting on a single particle (Figure 2a), we characterized the magnetic field near the tip

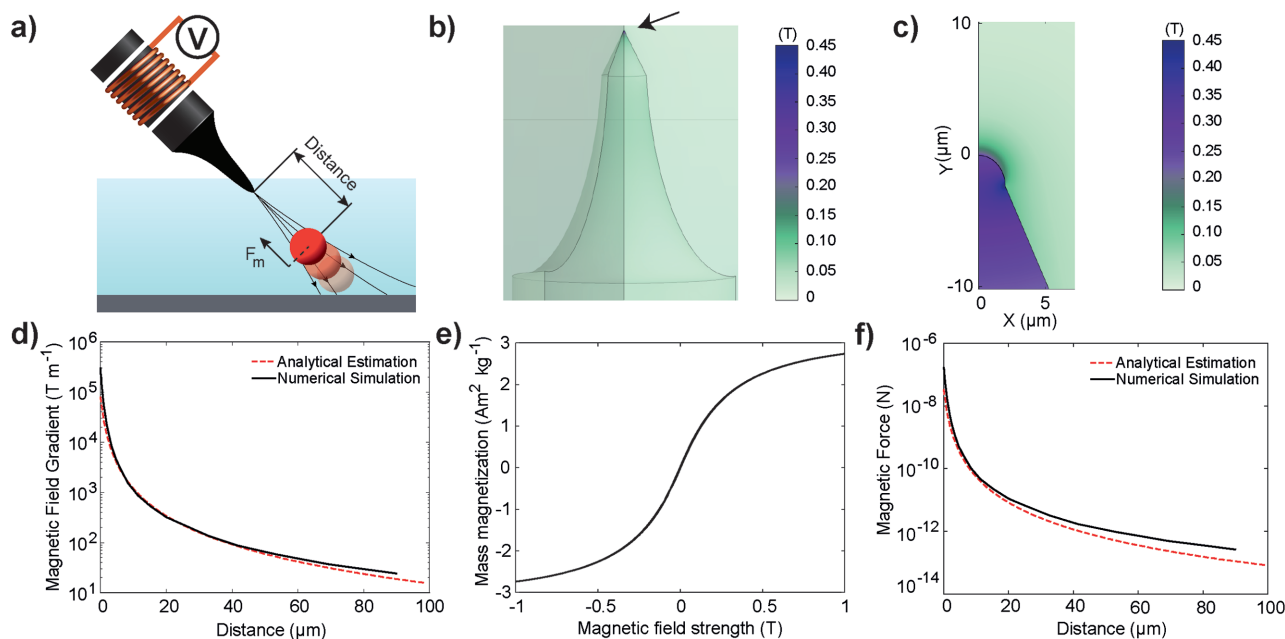


**Figure 2.** Magnetic characteristics of the system. a) Illustration of the components involved during the magnetophoretic pick-up. b) 3D view of the magnetic field saturation at the very tip of the needle emphasized with a black arrow. c) Close-up view of the 2D distribution of the magnetic field at the vicinity of the tip. d) Extrapolated magnetic field gradient of the needle for excitation coil current of 25 mA. The distance is measured from the tip of the needle. e) Mass magnetization of the superparamagnetic microparticles, measured using a vibrating sample magnetometer (VSM) at resolution of 1 mT. f) Estimated force–distance dependency between the needle tip and a single particle.

and the mass magnetization of the particles. Two types of magnetic characterization of the needle were carried out, numerical and analytical. The numerical simulation was performed within Comsol 5.2a (Experimental Section). The results from the numerical simulation show high concentration of the magnetic field at the very tip of the needle (Figure 2b), where a modest excitation current of 25 mA was applied, approximately an order of magnitude less than the current required to saturate the needle. A magnified view of the field distribution at the very tip of the needle is illustrated in Figure 2c.

The analytical estimation of the magnetic field of the needle was measured using a scanning tunneling junction (STJ) magnetic sensor (Experimental Section). The measured field strength was fitted using the least square method applying an inverse law previously reported for poled electromagnets.<sup>[40]</sup> From the fitted inverse law, the magnetic gradient  $\frac{dB}{d\delta} = \frac{dB}{dx} \frac{B_x}{B} + \frac{dB}{dy} \frac{B_y}{B} + \frac{dB}{dz} \frac{B_z}{B}$  ( $\delta$  is the distance from a single microparticle to the needle)<sup>[41]</sup> was estimated by computing the derivative of the fit (Experimental Section). The magnetic fields from the numerical simulation and analytical estimation are plotted in Figure 2d.

The mass magnetization  $M_p$  of a sample batch of our superparamagnetic microparticles was measured by a vibrating sample magnetometer (VSM) (Figure 2e and Experimental Section). The magnetic force acting on a single particle in a field  $B$  can then be expressed as

$$F_m = \frac{\pi}{6} d_p^3 \rho_p M_p B \frac{dB}{d\delta} \quad (1)$$

where  $d_p$  is the particle diameter, and  $\rho_p$  is the particle density. The estimated magnetic force acting on a single microparticle over a given distance based on the performed numerical simulation and analytical estimation is plotted in Figure 2f. For a supply current of 25 mA, the estimated force is up to  $\approx 700$  pN at the very tip of the needle. The force quickly drops to lower pico-Newton range after needle-to-particle distance becomes greater than 10  $\mu\text{m}$ . The derivation of the analytical estimation of the magnetophoretic force is elaborated in the Supporting Information.

### 2.3. Selective Picking

When two particles are close to each other during the picking phase, there is a risk of picking both particles at the same time. To avoid simultaneous picking, we first approach the targeted particle along the axis of the needle with minimized magnetic field gradient ( $\leq 100 \text{ T m}^{-1}$ ). When the needle is about 10–20  $\mu\text{m}$  away from the particle, picking is observed. Our experiments show that an individual particle can be picked up when the closest neighboring particle is at a distance of  $\approx 3 \mu\text{m}$ , as shown in Figure 3a–c and Video S2 (Supporting Information). A small disturbance to the neighboring particles has been observed, which does not impair the manipulation. We attribute the disturbance to both the influence of the magnetic field and the hydrodynamics caused by the motion of the particle picked.

We have also conducted a statistical study to determine the selectivity of the picking (Experimental Section). The picking success rate was determined using a weight function

$$(w = \sum_{i=1}^n \frac{V_i}{d_i^3}, V_i \text{ is the volume of the } i\text{th neighboring particle and}$$

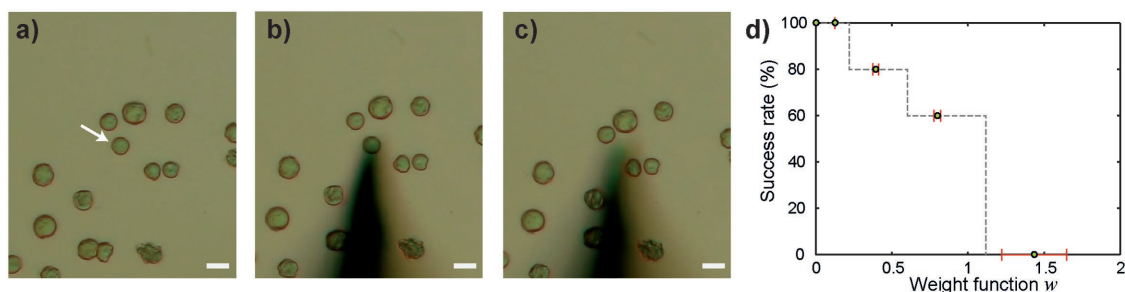


**Figure 3.** Selective picking of an individual particle from a population of particles. a) A population of particles in the given region-of-interest. The arrow denotes the targeted particle to be picked up. b) The magnetic field of the needle is minimized ( $\leq 100 \text{ T m}^{-1}$ ) and the pick-up occurs when the needle is sufficiently close to the particle (10–20  $\mu\text{m}$ ). c) The targeted particle has been picked up. Scale bars: 10  $\mu\text{m}$ . d) Statistical study on selectivity of the picking: success rate (%) over weight function  $w$ . The dashed line denotes the bin intervals, the dots denote the mean, and the error bars denote the variance of the weight function  $w$ , respectively.

$d_i$  is center-to-center distance between the targeted particle to the  $i$ th neighboring particle). The weight function was chosen because the magnetic force has a proportional representation  $F \sim \frac{V_i}{d_i^3}$  (see Equation (S6) in the Supporting Information); hence the weight function corresponds roughly with the total force acting on the particle population. Figure 3d shows that an individual particle can be selectively picked up with 100% success rate when the weight function for all the particles does not exceed 0.22, corresponding to a single neighboring particle being within a distance of less than 18  $\mu\text{m}$ . The pick-up success rate dropped to 80% when the range of the weight function was from 0.22 to 0.60. The pick-up success rate further dropped to 60% when the range of the weight function was from 0.60 to 1.12. Picking an individual particle completely failed when the weight function was higher than 1.12.

#### 2.4. Particle–Substrate/Needle Interaction during Particle Picking and Placing

We propose the following model for the interactions between the particle, the needle and the substrate during picking and placing. When an object is immersed in liquid, an electric double layer (EDL)<sup>[42,43]</sup> is formed around its surface. Before manipulation, the particles hover on top of the substrate due to repulsive interacting EDLs from the long Debye length for deionized water, resulting in significantly smaller particle-surface adhesion than the magnetic particle–needle attraction (Figure S1, Supporting Information). During the placement, a particle is placed by annulling the electrostatic repulsion between the particle and the substrate. EDL annulation can be done by pH regulation or by enforced molecular contact,<sup>[44]</sup> and in our case, we use the latter. Since the robotic positioner has a vertical loading capability several orders of magnitude higher than the repulsive layer, it can easily bring a single particle in contact with the substrate.

The placement can be explained by the adhesion process, as shown in **Figure 4**: (i) At the beginning of the placement, the radius of the contact area between the particle and the needle, and the particle and the substrate is denoted as  $a_{o-np}$  and  $a_{o-sp}$ , respectively, under the assumption that no extra load is applied ( $F = 0 \text{ N}$ ), both  $a_{o-np}$  and  $a_{o-sp}$  are on the ordinate in Figure 4b. (ii) Both contact areas increase when an external load is applied

from the needle by moving it toward the substrate. When the needle is retracted, the adhesion process is reversed. The adhesion process is not fully reversible, but involves energy dissipation (conversion of the kinetic energy to heat), that results in a hysteresis loop (Figure 4b). (iii) During the retraction, the radius of the interacting contact area shrinks even below the level of radius of the interacting contact area without external load  $a_o$ . Assuming elastic deformation, this radius miniaturization can occur up to the point when it reaches 63% of the radius of interacting contact area without external load,<sup>[45]</sup> known as radius of separation,  $a_s = a_o \cdot 4^{-1/3} = 0.63 \cdot a_o$ , with  $a_{s-sp}$  and  $a_{s-np}$  for substrate–particle and needle–particle, respectively. In our case, the radius of separation is first reached by the needle–particle curve, and a breakage occurs at that point, separating the needle and the particle. (iv) After separating from the needle, the particle remains on the substrate with a radius of remaining contact area denoted as  $a_{r-sp}$ . The final radius of the contact area between the particle and the substrate is the range between  $a_{r-sp}$  and  $a_{o-sp}$ . The above discussion is based on Johnson–Kendall–Roberts theory<sup>[45]</sup> of interacting elastic bodies.

The separation between the particle and the needle is attributed to the surface-to-particle adhesion being larger than the needle-to-particle adhesion during the separation process. The adhesion forces during the process, in general, are proportional to the effective radius  $R_{\text{eff}}$  and the interaction energy  $W$ , i.e.,  $F = 1.5R_{\text{eff}}W$ . On one hand, the effective radius of the substrate–particle is 2.7 times the effective radius of the needle–particle, and on the other hand, the needle–particle has 2.1 times higher interaction energy (0.083  $\text{J m}^{-2}$ ) with respect to the substrate–particle interaction energy (0.039  $\text{J m}^{-2}$ ), when they are all immersed in DI water. The effective radius is more dominant than the interaction energy for particles with radii greater than 1.4  $\mu\text{m}$ , i.e., the smallest particle than theoretically can be manipulated with this technique (theoretical estimation in Section 2 and Figure S2 in the Supporting Information).

#### 2.5. Transport Characterization

We characterize the high-speed positioning capability of the system by studying the reliability of the particle transport



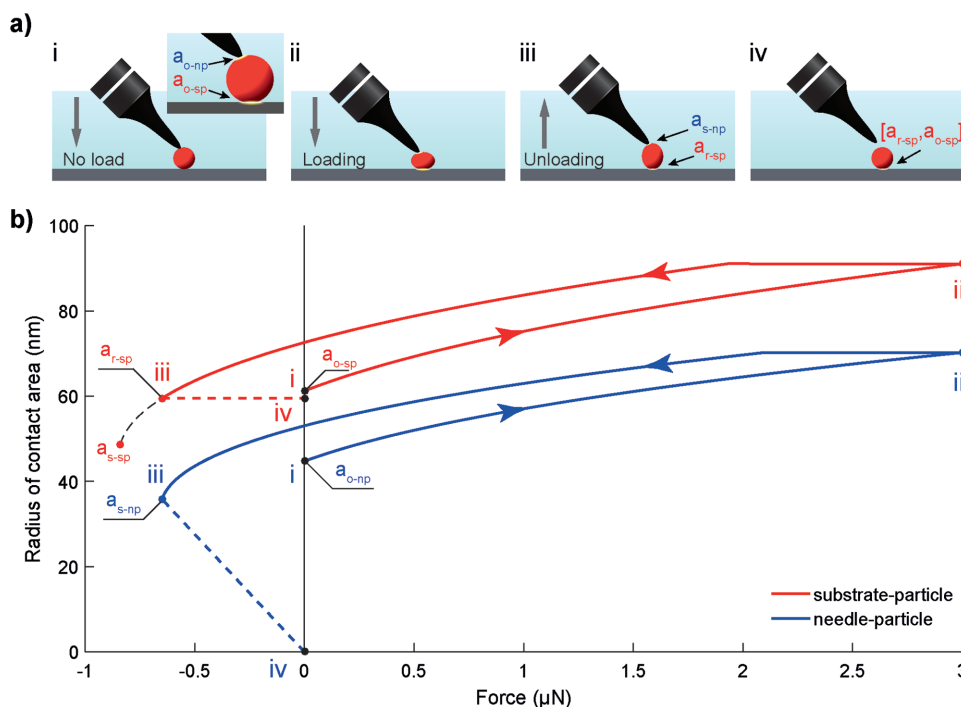


**Figure 4.** Principle of placing individual superparamagnetic microparticles with electromagnetic needle. Illustration not to scale. a) Schematic drawing of the placing phase of the manipulation method. (i) Microparticle brought into contact with the substrate under the assumption that no external load is compressing the particle. Inset: close-up illustration of initial radii of contact area between the needle–particle and substrate–particle, respectively. (ii) Particle–substrate contact enhanced by external load. (iii) Needle retraction up to a level of reaching radius of separation between the particle and the needle  $a_{s-np}$ , and radius of remaining contact area between the particle and the substrate  $a_{r-sp}$ . (iv) Needle fully retracted. Radius of contact area between the particle and the substrate is between the radius of remaining contact area and radius of interacting contact area without external load, i.e.,  $a_{r-sp}$  up to  $a_{o-sp}$ . b) Corresponding radius of contact area against the applied force on the schematically illustrated placing process depicted in (a).

at different moving speeds. During the transportation, a particle attached to the needle is subjected to a hydrodynamic drag directly proportional to the speed of the moving needle. Depending on the attraction force between the particle and the needle, the hydrodynamic drag can detach the particle from the needle during transportation. We observed a threshold magnetic attraction (coil excitation current of 18 mA resulting in estimated force of  $\approx 250$  pN) for reliable transportation: below the threshold, the maximum transportation velocity was  $\approx 65 \mu\text{m s}^{-1}$ ; above the threshold, robust transportation was observed at the highest possible positioning speed of the needle, i.e.,  $\approx 1.5 \text{ mm s}^{-1}$  (Figure S3 and Video S3, Supporting Information). We attribute this threshold magnetic attraction to breaking the repulsive EDL interaction which leads to a firm attachment.

## 2.6. Placing Characterization

Individual particles were picked and placed to quantitatively characterize the placing performance of the manipulation method in terms of accuracy and precision (Experimental Section). The distribution of the resulting placements is given in Figure S4 (Supporting Information). The calculated placing accuracy and precision are 0.34 and 0.85  $\mu\text{m}$ , respectively.

## 2.7. Line Formation, Patterning, Sorting, and 3D-Positioning

The application capability of this manipulation method has been experimentally investigated to determine: (1) the ability to place adjacent microparticles for highly condensed and continuous particle formations (e.g., lines), (2) scattered patterning of complicated shapes; (3) sorting of particles with different size and morphology; and (4) 3D positioning. To demonstrate continuous formations, we placed individual particles adjacently, forming a continuous line out of four particles (Figure 5a–d and Videos S4, Supporting Information). A subsequent particle can be placed while it is in contact with adjacent particle, resulting in a placement precision of 0.84  $\mu\text{m}$  in vertical axis and undetectable error in horizontal axis. For scattered patterning, our method can be used to create arbitrary patterns out of microparticles. Figure 5e shows a pattern made of 32 particles where each particle was carefully placed into a predefined pattern. Additionally, the method can be used for particle sorting based on size and morphology (Figure 5f). The particles were grouped in four categories, each of them into its own quadrant. In the quadrant (i), four spherical particles with mean diameter of 8.39  $\mu\text{m}$  were placed; quadrant (ii) contains spherical particles with a mean diameter of 6.56  $\mu\text{m}$ ; quadrant (iii) has two spherical particles with a mean diameter of 11.65  $\mu\text{m}$ ; and quadrant (iv) contains nonspherical particles with microscopically rough morphology.

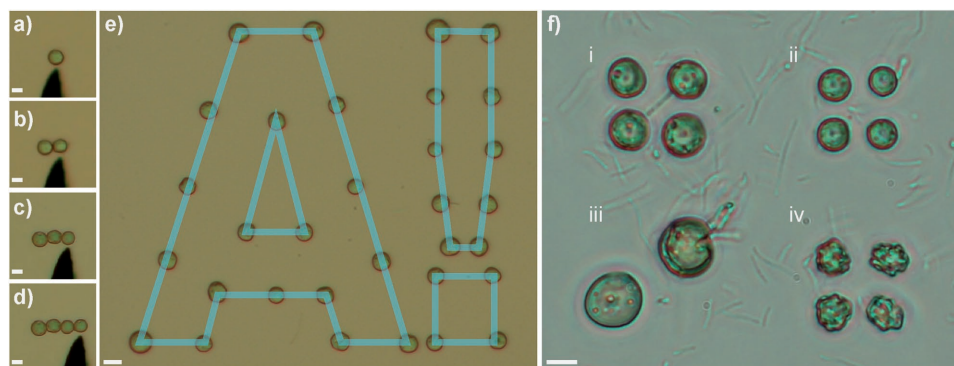


**Figure 5.** Placing capabilities and sorting as demo application. a–d) Placing four particles adjacently, no gap between two adjacent particles could be observed. e) Pattern creation (graphically enhanced). f) Separation of superparamagnetic microparticles based on size and morphology: (i) spherical particles with mean diameter of 8.39  $\mu\text{m}$ ; (ii) spherical particles with mean diameter of 6.56  $\mu\text{m}$ ; (iii) spherical particles with mean diameter of 11.65  $\mu\text{m}$ ; and (iv) nonspherical particles. Scale bars: 5  $\mu\text{m}$ .

We have also positioned particles on a 3D surface (Figure 6, Video S5 (Supporting Information), and Experimental Section). Initially, three superparamagnetic microparticles were randomly placed in the low segment of the trench-like 3D structure (Figure 6a). The needle approached and picked up the first microparticle (Figure 6b). Then, the needle was lifted up, transported the particle, and eventually placed the particle by touching it to the high segment of the structure (Figure 6c). The same procedure was repeated for the second and the third particle (Figure 6d–f).

Additionally, we have successfully manipulated a single polystyrene encapsulated iron-III-oxide (Microparticles GmbH, Germany) in DMEM cell culturing medium (General Electric, USA), Video S6 (Supporting Information).

### 3. Conclusion

This paper has presented a simple and highly deterministic manipulation technique for individual superparamagnetic microparticles. The ability to pick individual particles in a

population provides great flexibility in sample preparation where batch variances can be decreased, and multiple types of particles in a single experiment used. Placing individual particles in a population allows a great variety of applications where a large population of specimens, e.g., cells, are targeted. Since our needle is made of surgical grade stainless steel, it ensures compatibility with biomedical experimental studies. The robotic manipulation system can be automated to allow autonomous manipulation without a human operator to improve the performance even further.

### 4. Experimental Section

*Selective Picking Characterization:* 1  $\mu\text{L}$  of microparticles-in-water stock solution (concentration: 1  $\text{g L}^{-1}$ ) was mixed into DI water (100  $\mu\text{L}$ ) deposited onto a microscopic glass slide. Pick-up experimental trials started by the operator identifying a single particle and attempting to pick it up. If the targeted particle was picked together with other particles, then the trial was marked as a failure; if the targeted particle

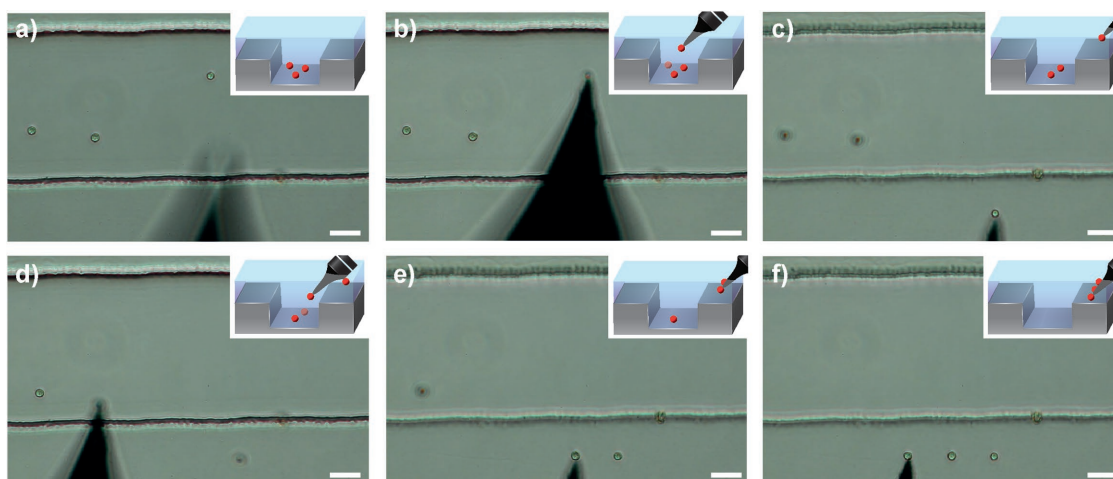


**Figure 6.** Manipulating microparticles on 3D structures. Insets illustrate the 3D position of each particle during the manipulation phase. a) Initial state: three particles suspended on the low segment within the trench-like pattern. b) Pick-up of the first particle from the low segment. c) Placing the first particle onto the high segment. d) Pick-up of the second particle from the low segment. e) Placing of the second particle onto the high segment. f) Placing the third particle onto the high segment. Scale bars: 20  $\mu\text{m}$ .

was picked alone, the trial was marked as a success. Twenty-five trials were carried out. A weight function  $\left(w = \sum_{i=1}^n \frac{V_i}{d_i^3}\right)$ , proportional to the magnetic force exerted on the particles, was used as the measure against the success rate of the selective picking, where  $V_i$  is the volume of the  $i^{\text{th}}$  neighboring particle and  $d_i$  is the center-to-center distance from the targeted to the neighboring  $i^{\text{th}}$  particle. Particles more than 18  $\mu\text{m}$  away from the targeted particle insufficiently contributed to the weight function and were excluded from the analysis.

**Placing Characterization:** A microscopic defect on the backside of the glass slide was visually identified as a reference mark. An overprint mark was placed on the computer monitor overlapping the reference mark. During manipulation experiments, the particle was placed at the overprint mark with best efforts. The centroids of the reference mark and the particle were identified by machine vision. The placement error was measured by calculating the difference between the identified centroids. Ten experimental trials were carried out. The accuracy and precision were calculated as mean and variance of the error, respectively, following ISO 5725-1 (Figure S4, Supporting Information).

**3D Positioning:** When picking, the needle approached the microparticles at a distance of 20–40  $\mu\text{m}$  before 25 mA current to the needle was applied. The current was switched off after a pick-up was observed. The needle was then lifted up for  $\approx 50 \mu\text{m}$ , moved toward a target position on the high segment and lowered toward it. Once the contact between the substrate and the particle was observed, the needle was lifted up.

**Fabrication of  $\text{Fe}_3\text{O}_4$ @HPMCAS Superparamagnetic Microparticles:** The  $\text{Fe}_3\text{O}_4$ @HPMCAS particles (1:1 mass ratio, or 1:4 volume ratio) were fabricated with microfluidic droplet based single emulsion flow focusing platform. The HPMCAS polymer (0.1 mg mL<sup>-1</sup>) and iron-III-oxide nanoparticles (0.1 mg mL<sup>-1</sup>) were mixed in ethyl acetate as inner flow and 2 (mg mL<sup>-1</sup>) poloxamer 407 was used as outer flow, with flow rates of 1 (mL h<sup>-1</sup>) and 20 (mL h<sup>-1</sup>), respectively. The droplets were collected in 2 (mg mL<sup>-1</sup>) poloxamer 407 and the ethyl acetate was removed by diffusion. The solidified particles were collected by centrifugation. The resulted microparticles have diameters varying from 3 up to 12  $\mu\text{m}$  (Figure S5, Supporting Information). During the manipulation experiments, spherical particles of sizes 6.3–7.3  $\mu\text{m}$  (determined by machine vision) were used.

**Fabrication of the Tip of Electromagnetic Needle:** 1 mm thick stainless steel (AISI 420) wire was chemically etched in 10% HCl–water solution. The wire was clamped between two tailor-made aluminum profiles attached to a linear DC motor M-122.2DD (Physik Instrumente, Germany). The voltage signals were generated by analog/digital–digital/analog (AD/DA) converter (NI 6351, National Instruments, USA). The signal was first amplified two times by an in-house developed voltage amplifier (LM358-N, Texas Instruments, USA), followed by a current amplification (BOP 100-4M, Kepco, USA). The current in the circuitry was monitored by a shunt resistor connected to the converter.

The etching process was divided into two phases. In the first phase, the wire was dipped into the 10% HCl–water solution for 3 mm at 5 V applied potential until 300 mA current drop was registered. In the second phase, the etched tip was redipped for 0.4 mm into the same solution at 16 V applied potential until the current dropped to 5 mA (Figure S6, Supporting Information). Finally, the tip was removed from the etching solution and cleaned in isopropanol, followed by DI water.

**Preparation of the Apparatus:** The apparatus is shown in Figure S7 (Supporting Information). The fabricated needle was coiled using an electric screwdriver. The coil contains 8–10 layers of copper wire (AWG 34), with more than 1000 coil turns in total, yielding overall resistance of  $\approx 10 \Omega$ . After coiling, the needle was attached to a hall sensor (SS495A1, Honeywell Inc., USA) using fast-acting cyanoacrylate glue (Super Glue, Loctite, USA), which was attached to a piezoelectric actuator (Pst 150 2  $\times$  3/5, Piezomechanik GmbH, Germany) following the same procedure. The piezoelectric actuator was also glued to an aluminum block (5  $\times$  10  $\times$  11 mm<sup>3</sup>). The block was fastened to the aluminum holder and the electromagnetic needle was tightened to the holder using a Teflon string. The holder, together with all other parts,

was fixed to the adapter, which was mounted to three degrees of freedom robotic nanopositioner (SLC1720, SmarAct GmbH, Germany). The whole apparatus was installed in an inverted microscope (Axio Vert. A1, Zeiss, Germany). The control of the positioner was realized by a control unit (MCS-3D, SmarAct GmbH, Germany). The driving voltage signals of the coil and the piezoelectric actuator were generated by the AD/DA converter (NI 6343, National Instruments, USA) connected to a personal computer. A 3.3  $\mu\text{F}$  capacitor was connected in parallel with the coil. The current to the coil was amplified by a linear amplifier (TS200, Accel Instruments, USA). A piezo linear amplifier (EPA-104, Piezo Systems Inc, USA) was used for voltage amplification of the piezoelectric actuator. An in-house developed software was used to execute user-defined scripts to move the robotic positioner, control the magnetic field of the coil, and vibrate the needle. A gamepad console (F710, Logitech, USA) was used for a human–machine interaction. The image and video acquisition was done by a digital single-lens reflex (DSLR) camera (EOS 550D, Canon, Japan), mounted onto the inverted microscope. During the manipulation experiments, 1–10  $\mu\text{L}$  of stock dispersion (particle concentration: 0.001–0.1 g L<sup>-1</sup>) was mixed into DI water (50–100  $\mu\text{L}$ ) in a chamber of a modified two-chamber glass slide (Lab-Tek, Thermo Fisher Scientific, USA).

**Characterization of Magnetic Moment of the Microparticles:** The magnetic moment of 2.45 mg bundle of  $\text{Fe}_3\text{O}_4$ @HPMCAS microparticles was measured in a multipurpose measurement system (PPMS Dynacool, Quantum Design, USA) using the VSM mode with an outer excitation magnetic field of  $\pm 1 \text{ T}$  with step size of 1 mT.

**Numerical Simulation of Magnetic Field and Field Gradient:** Magnetic field was numerically simulated within Comsol Multiphysics 5.2a (Comsol Group, Sweden). A 2D axisymmetric model was defined with geometry as close as possible to the real device. The chosen material type was AISI 416 stainless steel (nonlinear magnetic material) which has almost identical material content as the AISI 420 stainless steel, i.e., the material of the real needle. Stationary magnetic field study was used to generate the magnetic fields (line, planar, and 3D data) as well as field gradients. The magnetic field and field gradient data was exported to MATLAB (MathWorks, USA). The magnetization data of the particles was included in order to compute the magnetic force following the guidelines of Warnke<sup>[46]</sup> and Veeramachaneni and Carroll.<sup>[47]</sup>

**Analytical Estimation of Magnetic Field and Field Gradient:** During the magnetic characterization of the electromagnetic needle, the coil was placed onto a v-grooved aluminum piece and attached to the 3D robotic positioner. The v-grooved piece was used to align the needle and ensure its perpendicularity to the magnetic sensor (SpinT)-020, Micromagnetics, USA) (Figure S8a, Supporting Information). The needle was brought at  $\approx 2 \mu\text{m}$  from the sensor (Figure S8b, Supporting Information) and it was moved along the needle–sensor axis for 9 mm with step size of 1  $\mu\text{m}$  for 3 mm and remaining range of 6 mm with step size of 10  $\mu\text{m}$ . At each position, the needle was first demagnetized and the current was looped from 0 to 1 A. The magnetization at low current (1 mA) was extracted from the data and Equation (S1) in the Supporting Information was fitted with fitting coefficients:  $M_n = 58.58$  and  $4\beta = 10^6$ , returning a fit with 95% confidence level and goodness of the fit of  $R^2 = 0.75$ . The magnetic gradient was estimated by computing the derivative of the fit.

**Magnetic Field Control:** During teleoperation, the electromagnetic needle was controlled by changing the applied voltage with steps of 1 mA or setting the voltage to a desired value, usually 25 mA. The duration of the magnetization signal was either continuous or lasting for 100 ms. Demagnetization was achieved by sending sinusoidal decaying signal to the coil. The mathematical expression of the demagnetization signal is  $\gamma = \text{Amp} \sin(2\pi Ft + \varphi)e^{-at}$ , where *Amp* is the amplitude, *F* is sinusoidal frequency,  $\varphi$  is the phase shift, *a* is the attenuation factor, and *t* is the sampling period of (AD/DA) converter from which the signal was produced. Experimentally we have identified that the signal with *Amp* = 0.25 A, *F* = 20 Hz, *a* = 4, and *t* = 3.33  $\mu\text{s}$  demagnetizes the needle sufficiently; however, the needle cannot be completely demagnetized and some residual magnetism will always remain in the core.<sup>[48]</sup>

**Geometric Measurements of the Needle and the Particles:** The needle was horizontally placed onto its holder and brought to the field of view of the inverted microscope, and an image was acquired. A MATLAB script utilizing ready-made MATLAB function implanting Blob Tool algorithm was used. The radius of the needle was  $\approx 2 \mu\text{m}$ .

The average microparticle size was obtained through recording multiple images from a microparticle population. 50 microparticles for measuring were identified. The diameter for each particle was calculated utilizing a ready-made MATLAB function for finding circular shapes based on the Circular Hough Transform algorithm. The calculated mean diameter was  $6.9 \mu\text{m}$  with a standard deviation of  $0.5 \mu\text{m}$ .

**Electric Characterization of the Microparticles:** The zeta-potential of the microparticles was determined by filling 1 mL of stock dispersion (particle concentration:  $0.1 \text{ g L}^{-1}$ ) in a folded capillary cell within Zetaseizer Nano ZS90 (Malvern Instruments Corp, United Kingdom). The measurement was performed under ambient room temperature of  $25^\circ\text{C}$  and zeta-potential value was calculated by using the Smoluchowski equation.

**Microfabrication of Trench-Like 3D Microstructure:** The microfabrication processing was done on a microscope slide (VWR, USA). Initially, the slide was baked for 30 min at  $200^\circ\text{C}$  for dehumidization, followed by negative photoresist SU-8 50 (MicroChem Corp., USA) spin coating (4000 rpm, 30 s). After the SU-8 spin coating, the sample was post-baked for 8 min (automatically controlled temperature regimen: ramping from room temperature to  $65^\circ\text{C}$  for 3 min, steady baking at  $65^\circ\text{C}$  for 5 min, ramping from  $65$  to  $90^\circ\text{C}$  for 3 min, steady baking at  $90^\circ\text{C}$  for 40 min). When baking was over, the sample was left for 15 min relaxation in order to avoid sticking to the mask under soft contact mode within the mask aligner (SUSS MA6 MicroTec, Germany). Then, a black and white stripe pattern (black/white stripe width:  $100 \mu\text{m}$ ) was exposed for 16 s under UV light. After the exposure, the sample was brought to post-exposure baking (automatically controlled temperature regimen: ramping from room temperature to  $90^\circ\text{C}$  for 5 min, steady baking at  $90^\circ\text{C}$  for 40 min, ramping from  $90^\circ\text{C}$  to room temperature for 15 min) followed by resist strip off in SU-8 developer (MR-600, MicroChem Corp, USA) for 10 min. Finally, the sample was cleaned using isopropanol.

**Microscopic Imaging:** During the manipulation experiments of the superparamagnetic microparticles, the image and video were acquired by a DSLR camera (EOS 550D, Canon, Japan) mounted on the inverted microscope (Axio Vert.A1, Zeiss, Germany). In placing characteristics and pattern creating experiments (Figure 5a–e), a neutral-density filter was used for obtaining higher particle-to-background contrast. In the sorting experiment (Figure 5f) and the manipulation on 3D structures (Figure 6), phase contrast (PH) filter was used for illustrating differences in morphology as well as having a great depth of field for showing out-of-focus objects.

The SEM images of the needle were taken by an Environmental Scanning Electron Microscope (EVO HD15, Zeiss, Germany). The SEM image of the microparticles was also taken by a Field Emission Gun Scanning Electron Microscope (Quanta 250, FEI, USA). The TEM images of the microparticles were taken by JEM 1400 (Jeol, USA) transmission electron microscope. The transmission electron micrographs were imaged using a JEM 1400 (JEOL Ltd., Japan) operating at 80 kV acceleration voltage and equipped with a Gatan Orius SC 1000B CCD camera (Gatan Inc., USA). The microparticle sample was dried overnight at  $50^\circ\text{C}$ , embedded into epoxy TAAB 812 (TAAB, UK), and cured for 14 h at  $60^\circ\text{C}$ . Finally, thin sections of 60–90 nm thickness were cut at room temperature using an ultramicrotome Leica ultracut UCT (Leica Mikrosysteme GmbH, Austria) and transferred on copper grids.

## Supporting Information

Supporting Information is available from the Wiley Online Library or from the author.

## Acknowledgements

This research work was supported by the Academy of Finland (projects #304843, #295006, #298635, #252215, #281300, #292477, and #299087), Aalto University School of Electrical Engineering, University of Helsinki Research Funds, the Biocentrum Helsinki, the European Research Council under the European Union's Seventh Framework Programme (FP/2007-2013, grant no. 310892), and Jane and Aalto Foundation (Grant no. 4704010). The authors thank the Electron Microscopy Unit of the Institute of Biotechnology, University of Helsinki, and Micronova Nanofabrication Center for providing laboratory facilities for imaging and microfabrication. Authors would also like to express their gratitude to S. Nurmi for insightful feedback on design and manufacturing of the mechanical parts, to V. Jokinen for contributions to the microfabrication process of the trench-like structure, to V. Liimatainen and J. Timonen for fruitful discussion and feedback, as well as to A. Siddiqi for proofreading the manuscript.

## Conflict of Interest

The authors declare no conflict of interest.

## Keywords

electromagnetic needles, individual, manipulation, superparamagnetic microparticles

Received: July 6, 2017

Revised: August 19, 2017

Published online: October 16, 2017

- [1] D. K. Schweizer, E. K. Eigler, *Nature* **1990**, *344*, 524.
- [2] M. Sitti, *IEEE/ASME Trans. Mechatronics* **2000**, *5*, 199.
- [3] Q. Zhou, P. Korhonen, J. Laitinen, S. Sjoval, *J. Micromechanics* **2006**, *3*, 359.
- [4] A. Ashkin, J. M. Dziedzic, J. E. Bjorkholm, S. Chu, *Opt. Lett.* **1986**, *11*, 288.
- [5] A. Martinez, H. C. Mireles, I. I. Smalyukh, *Proc. Natl. Acad. Sci. USA* **2011**, *108*, 20891.
- [6] H. Xu, S. Jones, B. C. Choi, R. Gordon, *Nano Lett.* **2016**, *16*, 2639.
- [7] A. H. B. De Vries, J. S. Kanger, B. E. Krenn, R. Van Driel, *J. Microelectromechanical Systems* **2004**, *13*, 391.
- [8] J. V. I. Timonen, A. F. Demirörs, B. A. Grzybowski, *Adv. Mater.* **2016**, *28*, 3453.
- [9] X. Ding, S.-C. S. Lin, B. Kiraly, H. Yue, S. Li, I.-K. Chiang, J. Shi, S. J. Benkovic, T. J. Huang, *Proc. Natl. Acad. Sci. USA* **2012**, *109*, 11105.
- [10] Q. Zhou, V. Sariola, K. Latifi, V. Liimatainen, *Nat. Commun.* **2016**, *7*, 1.
- [11] M. Dürr, J. Kentsch, T. Müller, T. Schnelle, M. Stelzle, *Electrophoresis* **2003**, *24*, 722.
- [12] J. P. Xu, K. J. Kwak, J. L. Lee, G. Agarwal, *Small* **2010**, *6*, 2105.
- [13] B. Lim, V. Reddy, X. Hu, K. Kim, M. Jadhav, R. Abedini-Nassab, Y.-W. Noh, Y. T. Lim, B. B. Yellen, C. Kim, *Nat. Commun.* **2014**, *5*, 3846.
- [14] L. Johansson, K. Gunnarsson, S. Bijelovic, K. Eriksson, A. Surpi, E. Göthelid, P. Svedlindh, S. Oscarsson, *Lab Chip* **2010**, *10*, 654.
- [15] H. Lee, a. M. Purdon, R. M. Westervelt, *Appl. Phys. Lett.* **2004**, *85*, 1063.



- [16] B. B. Yellen, R. M. Erb, H. S. Son, R. Hewlin Jr., H. Shang, G. U. Lee, *Lab Chip* **2007**, *7*, 1681.
- [17] D. Holzinger, D. Lengemann, F. G?llner, D. Engel, A. Ehresmann, *Appl. Phys. Lett.* **2012**, *100*, 153504.
- [18] L. Lagae, R. Wirix-Speetjens, J. Das, D. Graham, H. Ferreira, P. P. F. Freitas, G. Borghs, J. De Boeck, *J. Appl. Phys.* **2002**, *91*, 7445.
- [19] K. S. Kim, J.-K. Park, *Lab Chip* **2005**, *5*, 657.
- [20] T. Ueltzhöffer, R. Streubel, I. Koch, D. Holzinger, D. Makarov, O. G. Schmidt, A. Ehresmann, *ACS Nano* **2016**, *10*, 8491.
- [21] Q. Ramadan, D. P. Poenar, C. Yu, *Microfluidic Nanofluidics* **2009**, *6*, 53.
- [22] C. P. Gooneratne, O. Yassine, I. Giouroudi, J. Kosel, *IEEE Trans. Magn.* **2013**, *49*, 3418.
- [23] E. Mirowski, J. Moreland, S. E. Russek, M. J. Donahue, *Appl. Phys. Lett.* **2004**, *84*, 1786.
- [24] D. Holzinger, I. Koch, S. Burgard, I. N. Science, *ACS Nano* **2015**, *1111*, 1.
- [25] T. Deng, G. M. Whitesides, M. Radhakrishnan, G. Zabow, M. Prentiss, *Appl. Phys. Lett.* **2001**, *78*, 1775.
- [26] M. Donolato, P. Vavassori, M. Gobbi, M. Deryabina, M. F. Hansen, V. Metlushko, B. Ilic, M. Cantoni, D. Petti, S. Brivio, R. Bertacco, *Adv. Mater.* **2010**, *22*, 2706.
- [27] M. Monticelli, E. Albisetti, D. Petti, D. V. Conca, M. Falcone, P. P. Sharma, R. Bertacco, *J. Appl. Phys.* **2015**, *117*, 17B317.
- [28] M. Monticelli, A. Torti, M. Cantoni, D. Petti, E. Albisetti, A. Manzin, E. Guerriero, R. Sordan, G. Gervasoni, M. Carminati, G. Ferrari, M. Sampietro, R. Bertacco, *Small* **2015**, *12*, 921.
- [29] B. D. Matthews, D. A. LaVan, D. R. Overby, J. Karavitis, D. E. Ingber, *Appl. Phys. Lett.* **2004**, *85*, 2968.
- [30] M. Barbic, J. J. Mock, A. P. Gray, S. Schultz, *Appl. Phys. Lett.* **2001**, *79*, 1897.
- [31] J. H. Lee, J. W. Kim, M. Levy, A. Kao, S. H. Noh, D. Bozovic, J. Cheon, *ACS Nano* **2014**, *8*, 6590.
- [32] K. Gunnarsson, P. E. Roy, S. Felton, J. Pihl, P. Svedlindh, S. Berner, H. Lidbaum, S. Oscarsson, *Adv. Mater.* **2005**, *17*, 1730.
- [33] B. Riedmüller, B. Sarma, N. Hibst, U. Herr, *IEEE Trans. Magn.* **2014**, *50*, 1.
- [34] F. Amblard, B. Yurke, A. Pargellis, S. Leibler, *Rev. Sci. Instrum.* **1996**, *67*, 818.
- [35] L. Sacconi, G. Romano, R. Ballerini, M. Capitanio, M. De Pas, M. Giuntini, D. Dunlap, L. Finzi, F. S. Pavone, *Opt. Lett.* **2001**, *26*, 1359.
- [36] Z. Zhou, H. Miller, A. Wollman, M. Leake, *Photonics* **2015**, *2*, 758.
- [37] J. K. Fisher, J. R. Cummings, K. V. Desai, L. Vicci, B. Wilde, K. Keller, C. Weigle, G. Bishop, R. M. Taylor, C. W. Davis, R. C. Boucher, E. T. O'Brien, R. Superfine, *Rev. Sci. Instrum.* **2005**, *76*, 53711.
- [38] D. Matsuura, H. Aoki, Y. Takeda, in *IEEE Int. Conf. Robotics and Automation* IEEE, Stockholm, Sweden **2016**, p. 1745.
- [39] H. Zhang, D. Liu, M. A. Shahbazi, E. Mäkilä, B. Herranz-Blanco, J. Salonen, J. Hirvonen, H. A. Santos, *Adv. Mater.* **2014**, *26*, 4497.
- [40] A. H. B. De Vries, B. E. Krenn, R. Van Driel, J. S. Kanger, *Biophys. J.* **2005**, *88*, 2137.
- [41] D. F. Bagster, *Int. J. Miner. Process.* **1987**, *20*, 1.
- [42] B. Derjaguin, L. Landau, *Acta Physicochim. URSS* **1941**, 633.
- [43] E. J. W. Verwey, *J. Phys. Colloid Chem.* **1947**, *51*, 631.
- [44] J. N. Israelachvili, *Intermolecular and Surface Forces*, Elsevier **2011**.
- [45] K. L. Johnson, K. Kendall, A. D. Roberts, *Proc. R. Soc. London, Ser. A* **1971**, *324*, 301.
- [46] K. C. Warnke, *IEEE Trans. Magn.* **2003**, *39*, 1771.
- [47] U. K. Veeramachaneni, R. L. Carroll, presented at Proc. COMSOL Conf., Boston, USA, March **2009**.
- [48] B. D. Cullity, C. D. Graham, *Introduction to Magnetic Materials*, John Wiley & Sons, Hoboken, New Jersey, USA **2011**.